Ion Transport and Vibrational Spectra of Branched Polymer and Dendrimer Electrolytes

Rensl E. A. Dillon and Duward F. Shriver*

Department of Chemistry and Materials Research Center, Northwestern University, Evanston, Illinois 60208-3113

Received November 9, 2000. Revised Manuscript Received January 18, 2001

Solid electrolytes were prepared by the introduction of $Li[(CF_3SO_2)_2N]$ into amorphous branched polymers and dendritic macromolecular hosts. These materials exhibit high ionic conductivity, but high concentrations of salt increase the glass transition temperatures, with an attendant decrease in ionic conductivity.

Introduction

Armand and co-workers were the first to recognize the potential applications of polymer electrolytes in electrochemical devices such as batteries and electrochromic windows.[1] Polymer electrolytes are attractive because their high compliance promotes contact with the electrodes.[2,3] In early studies, it was postulated that cation transport occurs by ion hopping along the interior of the crystalline PEO helix;[4] however, it was later demonstrated that amorphous regions of the polymer salt complex exhibit the highest conductivity.[5,6]

Subsequent research suggests that segmental motion of the polymer promotes ion transport by making and breaking the coordination sphere of the solvated ion.[7] The concept that ion motion is coupled with the structural relaxations of the polymer is supported by evidence such as the poor conductivity of the electrolyte below the glass transition temperature, where the segmental motion of the polymer is largely frozen. An example of an effective polymer host is poly(bis-(2-(2-methoxy ethoxy)ethoxy)phosphazene) (MEEP), which consists of a highly flexible poly(phosphazene) backbone with short polyether side chains.[8]

In the present research, we explored polar dendritic macromolecules (also known as cascade macromolecules) or hyperbranched polymers as the host for ions. Dendrimers are characterized by highly branched polymer chains emanating from a central core, and they contain a large number of chain ends.[9,10] Dendrimers of lower generation contain fewer branching units and adopt flat ellipsoidal structures, whereas higher-generation dendrimers are more nearly spherical. Dendrimers have recently been used in a variety of applications such as encapsulating agents[11] and magnetic resonance imaging contrast agents,[12] hosts for combinatorial chemistry,[13] and coating materials.[14]

The noncrystalline nature of some dendrimers makes them attractive as the host for electrolytes. In addition, these branched polymers contain a large number of chain ends, which should result in a high free volume and low glass transition temperatures.[15,16] Dendrimers containing benzene and ethylene oxide groups in the chain branches have been used as hosts for ions in solid electrolytes;[17,18] however, the rigid phenyl groups in those dendrimers resulted in high glass transition temperatures for the salt complex. In the present research, amine dendrimers such as poly(propyleneimine) tetrahexacontaamine dendrimer (DAB-AM-64) (Figure 1) and starburst poly(amidoamine) (PAMAM) (Figure 2) were chosen for study because they do not contain rigid groups. These ion-doped dendrimers are compared to analogous branched poly(ethylenimine) ($-NHCH_2CH_2N-H_2-)_x[N(CH_2CH_2NH_2)CH_2CH_2-]_y-$BPEI) which has been studied as a host for polymer electrolyte materials.[19,20]

Experimental Section

Materials. $Li[(CF_3SO_2)_2N]$ (3 M) was dried on a high vacuum line at 150 °C for 2 days (8×10^{-6} Torr) and then

(1) Armand, M. B.; Chabagno, J. M.; Duclot, M. J. In *Fast Ion Transport in Solids Electrodes and Electrolytes*; Vashishta, P., Mundy, J. N., Shenoy, G. K., Eds.; Elsevier North-Holland, Inc.: Lake Geneva, Switzerland, 1979.
(2) Gray, F. M. *Solid Polymer Electrolytes: Fundamentals and Technological Applications*; VCH Publishers: New York, 1991.
(3) Ratner, M. A.; Shriver, D. F. *Chem. Rev.* **1988**, *88*, 109.
(4) Armand, M. *Solid State Ionics* **1983**, *9−10*, 745.
(5) Stainer, M.; Hardy, L. C.; Whitmore, D. H.; Shriver, D. F. *J. Electrochem. Soc.* **1984**, *131*, 784.
(6) Berthier, C.; Gorecki, W.; Minier, M.; Armand, M. B.; Chabagno, J. M.; Rigaud, P. *Solid State Ionics* **1983**, *11*, 91.
(7) Ratner, M. A. In *Polymer Electrolyte Reviews*; MacCallum, J. R., Vincent, C. A., Eds.; Elsevier Applied Science: New York, 1987; Vol. 1.
(8) Blonsky, P. M.; Shriver, D. F.; Austin, P.; Allcock, H. R. *J. Am. Chem. Soc.* **1984**, *106*, 6854.
(9) Zeng, F.; Zimmerman, S. C. *Chem. Rev.* **1997**, *97*, 1681.
(10) Fischer, M.; Vogtle, F. *Angew. Chem., Int. Ed. Engl.* **1999**, *38*, 884.
(11) Hawker, C. J.; Wooley, K. L.; Frechet, J. M. J. *J. Chem. Soc., Perkin Trans. 1* **1993**, *21*, 1287.
(12) Weinmann, H. J.; Ebert, W.; Misselwitz, B.; Raduchel, B.; Schmitt-Willich, H.; Platzek, J. *Eur. Radiol.* **1997**, *7*, 196.
(13) Kim, R. M.; Manna, M.; Hutchins, S. M.; Griffin, P. R.; Yates, N. A.; Bernick, A. M.; Chapman, K. T. *Proc. Natl. Acad. Sci. U.S.A.* **1996**, *93*, 10012.
(14) Wells, M.; Crooks, R. M. *J. Am. Chem. Soc.* **1996**, *118*, 3988.
(15) Takagishi, T.; Okuda, S.; Kuroki, N.; Kozuka, H. *J. Polym. Sci., Polym. Chem.* **1985**, *23*, 2109.
(16) Wooley, K. L.; Hawker, C. J.; Pochan, J. M.; Frechet, J. M. J. *Macromolecules* **1993**, *26*, 1514.
(17) Wang, Z.; Ikeda, M.; Hirata, N.; Kubo, M.; Itoh, T.; Yamamoto, O. *J. Electrochem. Soc.* **1999**, *146*, 2209.
(18) Hawker, C. J.; Chu, F.; Pomery, P. J.; Hill, D. J. T. *Macromolecules* **1996**, *29*, 3831.
(19) Harris, C. S.; Ratner, M. A.; Shriver, D. F. *Macromolecules* **1987**, *20*, 1778.
(20) Paul, J.-L.; Jegat, C.; Lassegues, J.-C. *Electrochim. Acta* **1992**, *37*, 1623.

10.1021/cm0008866 CCC: $20.00
Published on Web 03/09/2001

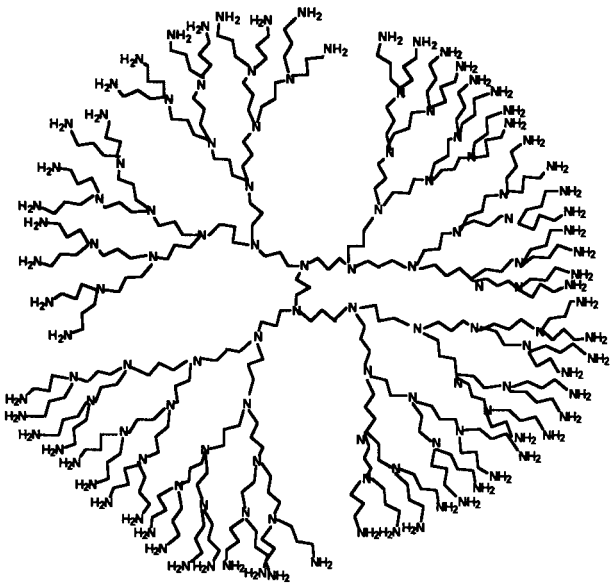

Figure 1. Two-dimensional structural representation of the dendrimer DAB-AM-64.

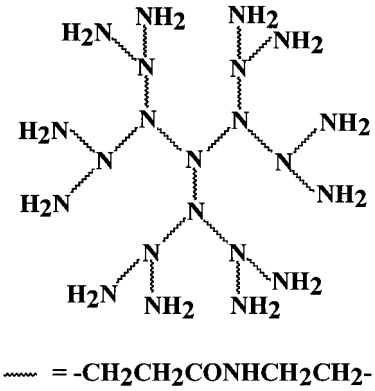

Figure 2. Schematic of a generation 2 starburst PAMAM dendrimer.

handled in a drybox. The dendrimer DAB-AM-64 (Aldrich, generation 5.0, M_w = 7169) contains 64 primary amines on its surface. The glass transition temperature is −84 °C. This material was dried under vacuum at 50 °C (1×10^{-1} Torr) for 1 day and then at 40 °C (8×10^{-6} Torr) for 2 days. The PAMAM dendrimer (Aldrich, generation 4, 10 wt % solution in methyl alcohol, M_n = 14 215) has 64 primary amino groups on its surface. This material was dried under vacuum at 50 °C (1×10^{-1} Torr) for 1 day and then at 80 °C (8×10^{-6} Torr) for 2 days. The branched polymer BPEI (Aldrich), which has M_n = 10 000 (determined by gel permeation chromatography) and M_w = 25 000 (determined by light scattering) was dried under vacuum at 50 °C (1×10^{-1} Torr) for 1 day and then at 40 °C (8×10^{-6} Torr) for 2 days. Tetrahydrofuran (THF) was distilled under nitrogen from sodium benzophenone.

Complex Formation. Dried and outgassed materials were manipulated under an inert atmosphere of dry nitrogen. Salt complexes were prepared by adding THF to appropriate molar quantities of $Li[(CF_3SO_2)_2N]$ and the dendrimer DAB-AM-64. Similar procedures were followed for the preparation of complexes of $Li[(CF_3SO_2)_2N]$/PAMAM, and $Li[(CF_3SO_2)_2N]$/BPEI. Small molecule solvents were then removed from the homogeneous polymer-salt solutions under vacuum at 50 °C (1×10^{-1} Torr) for a day, followed by 40 °C (8×10^{-6} Torr) for 2 days.

Physical Characterization. Differential scanning calorimetry (DSC) was performed on a Perkin-Elmer Pyris 1 instrument on samples loaded in hermetically sealed aluminum pans. A stable baseline was observed over the temperature range −100 to 200 °C, and the instrument was calibrated using indium and decane. Heating rates of 40, 20, and 10 °C/cm resulted in transition temperatures for representative samples that randomly varied by 5−8 °C; all transitions were recorded at a heating rate of 40 °C/min. Glass transitions were assigned at the middle of the transition. Melting and cold crystallization temperatures were assigned to the onset of the transitions. Amorphous materials exhibited a glass transition as the only thermal transition in the first DSC scan (not melt quenched). Crystalline samples were melted and subsequently quenched to −100 °C at 200 °C/min in an attempt to form amorphous materials. The DSC scan after quenching displayed the following thermal transitions: T_c (cold crystallization), T_g* (glass transition after quenching), and T_m* (melting point after quenching).

Table 1. DSC Data[a] for Macromolecular Complexes of DAB-AM-64, PAMAM-G4-64, and BPEI Doped with $Li[(CF_3SO_2)_2N]$

complexes[b]	T_g	T_m	T_g*
DAB-AM-64/$Li[(CF_3SO_2)_2N]$	−64		
17:1	−36		
9:1	−8		
4.5:1	27		18
BPEI/$Li[(CF_3SO_2)_2N]$	−46		
29:1	−34		
15:1	−23		
4:1	30		28
PAMAM-G4-64/$Li[(CF_3SO_2)_2N]$	7		
9:1		41	23
5:1		49	44
1:1		42	40

[a] T_g (°C) = glass transition temperature, T_g* (°C) = glass transition temperature after quenching, T_m (°C) = melting temperature, T_m* (°C) = melting temperature after quenching, T_c (°C) = cold crystallization temperature, and T_c* (°C) = cold crystallization temperature after quenching. [b] Macromolecule repeat units are used to calculate macromolecule/salt ratios.

Raman spectra were recorded on a FT-Raman spectrometer with excitation by a Nd:YAG laser at 1.064 μm. Samples in capillary tubes were probed in the 180° backscattering geometry. Amorphous samples exhibited weaker and broader bands in comparison to the sharper spectra of the crystalline samples. The resolution of the interferometer was 4 cm^{-1}.

Infrared spectra were recorded on a Bomem MB-100 FTIR spectrometer at 2 cm^{-1} resolution. Amorphous samples were placed between KBr plates and transferred under N_2. Crystalline samples were prepared as Nujol mulls.

Complex impedance measurements were performed with a Hewlett-Packard 4192A instrument in the frequency range 5 Hz to 13 MHz on samples sandwiched between stainless steel electrodes and annealed for 12−24 h at 100 °C before data collection. The apparatus was periodically calibrated. Data were recorded at 10 °C intervals as samples were cycled between 100 and 20 °C using a temperature ramp of 0.2 °C/min.

Results and Discussion

Thermal Analysis. The dissolution of $Li[(CF_3SO_2)_2N]$ into DAB-AM-64 in varying ratios results in the formation of amorphous complexes. Glass transition temperatures (Table 1) increase linearly with increasing salt concentration. This trend is attributed to the inhibition of segmental motion by coordination between the lithium cation and the amine groups of the dendrimer.[21] Similarly, incremental dissolution of $Li[(CF_3SO_2)_2N]$ into BPEI resulted in the formation of a series of amorphous complexes that exhibited increasing glass transition temperatures with increasing salt concentra-

(21) Popall, M.; Durand, H. *Electrochim. Acta* **1992**, *37*, 1593.

Table 2. Raman Frequencies and Vibrational Assignments for Li[$(CF_3SO_2)_2N$] (LiTFSI) Branched and Hyperbranched Polymer Complexes[a] (700−1300 cm^{-1})

Raman[b]	LiTFSI	A[c]	B[c]	C	D	E	F	G	H	I
ν_s CF_3 (s)	1247			1244	1242	1242	1243	1242	1242	1245
ν_s SO_2 (m)	1131			1139	1137	1139	1138	1135	1135	1138
δ_s CF_3 (vs)	747	740	743	742	741	742	742	742	742	746

[a] (A) Li[$(CF_3SO_2)_2N$]/BPEI = 1:29. (B) Li[$(CF_3SO_2)_2N$]/BPEI = 1:15. (C) Li[$(CF_3SO_2)_2N$]/BPEI = 1:4. (D) Li[$(CF_3SO_2)_2N$]/DAB-AM-64 = 1:17. (E) Li[$(CF_3SO_2)_2N$]/DAB-AM-64 = 1:9. (F) Li[$(CF_3SO_2)_2N$]/DAB-AM-64 = 1:4. (G) Li[$(CF_3SO_2)_2N$]/PAMAM = 1:9. (H) Li[$(CF_3SO_2)_2N$]/PAMAM = 1:5. (I) Li[$(CF_3SO_2)_2N$]/PAMAM = 1:1. [b] Assignments: v (stretching), δ (bending). The subscript s denotes symmetric motions. Band intensities: vs (very strong), s (strong), m (medium). [c] Bands of ν_s CF_3 and ν_s SO_2 are hidden by strong bands of BPEI.

tions. Elevation of the glass transition temperature occurs with increasing salt content in the DAB-AM-64 complexes, but this phenomenon was less pronounced than it was for BPEI complexes. Theoretical studies by Druger and co-workers indicate that the primary nitrogens on the periphery of a dendrimer are the primary sites for coordination of the metal cations,[22] and as a result, chain-end fluctuations are restricted upon formation of the dendrimer salt complex, with a concomitant increase in the glass transition temperature of the material. BPEI has a lower concentration of primary amines than DAB-AM-64, and this difference might explain the different glass transition temperatures for complexes of these two materials.

In contrast to the findings for the DAB-AM-64 and BPEI complexes, the introduction of Li[$(CF_3SO_2)_2N$] into PAMAM results in the formation of crystalline phases (Table 1). However, an amorphous electrolyte is formed when the molten PAMAM complex is quenched. Coordination of the lithium cation to the interior and the periphery of the dendrimer should result in significant inhibition of dendritic segmental motion and formation of a crystalline phase. Accordingly, the PAMAM/Li[$(CF_3SO_2)_2N$] (1:1) complex displays a lower melting point and glass transition temperature for the quenched material than does PAMAM/Li[$(CF_3SO_2)_2N$] (5:1).

Raman Spectroscopy of Anion Modes. The strongest band in the Raman spectrum of Li[$(CF_3SO_2)_2N$] is assigned as a symmetric deformation mode, δ_s CF_3, at 747 cm^{-1}.[23] Complexes of this salt with DAB-AM-64, PAMAM, and BPEI shift this deformation mode into the range 740−743 cm^{-1} (Table 2). These shifts are analogous to those reported by Rey and co-workers for Li[$(CF_3SO_2)_2N$] in poly(ethylene oxide) (PEO).[24] Similarly, the Raman bands for ν_s CF_3 and ν_s SO_2 of Li[$(CF_3SO_2)_2N$] in PEO[24] are analogous to the ν_s CF_3 and ν_s SO_2 Raman bands in Table 2 for Li[$(CF_3SO_2)_2N$] complexes with DAB-AM-64, PAMAM, and BPEI.

FTIR Investigation of Anion−Cation Interactions The shifts in the anion modes of Li[$(CF_3SO_2)_2N$] (Table 3) are similar to those observed by Rey and coworkers for Li[$(CF_3SO_2)_2N$] in poly(ethylene oxide).[25] The asymmetric stretching frequency of the S−O group is split into two bands at 1352 and 1333 cm^{-1} when the salt is dissolved in BPEI or DAB-AM-64. These distinct frequencies indicate that the dissociation of the cation from the anion is substantial.

The N−H and C−H stretching frequencies are listed in Table 4 for BPEI and DAB-AM-64 complexes with Li[$(CF_3SO_2)_2N$]. The primary amino groups in BPEI give rise to asymmetric and symmetric N−H stretching bands at 3351 and 3282 cm^{-1}, respectively (a shoulder at 3196 cm^{-1} is likely an overtone of the NH_2 deformation at 1599 cm^{-1}).[26] The symmetric N−H stretching vibration of the secondary amine is a weak band at (3282 cm^{-1}), and the symmetric N−H stretch is stronger than that of primary amines. The symmetric and asymmetric N−H stretching frequencies are lower than those of the corresponding (free) hydrogen-bonded amines.[27]

Harris reported that the N−H stretching bands of BPEI shift to higher frequencies when it is doped with $NaSO_3CF_3$.[19] This shift is attributed to solvation of the cation by the amine group, which frustrates hydrogen bonding with lone pairs on the nitrogen atom. Similarly, the asymmetric and symmetric N−H stretching frequencies shift to higher frequency when BPEI is doped with Li[$(CF_3SO_2)_2N$]. At Li[$(CF_3SO_2)_2N$]/BPEI ratios of 1:15 and 1:4, the symmetric N−H band splits into two bands.

The infrared spectrum of the dendrimer DAB-AM-64 contains an asymmetric N−H stretching band at 3362 cm^{-1}, which is approximately 10 cm^{-1} higher than the analogous band in BPEI. However, the symmetric N−H stretching frequencies of DAB-AM-64 and BPEI are similar. DAB-AM-64 salt complexes with Li[$(CF_3SO_2)_2N$] display infrared spectra that are substantially different from those of the BPEI complexes. As the salt concentrations increase, the asymmetric N−H frequency of the DAB-AM-64 salt complexes decreases to about 3352 cm^{-1} and then slowly increases, but the shift is not as pronounced as that seen for the BPEI complexes. The symmetric N−H frequencies of DAB-AM-64 split into three peaks on complex formation.

Unlike BPEI and DAB-AM-64, which solvate the lithium cation by primary and secondary amine groups, the dendrimer PAMAM solvates cations by interior amide groups, H−N−C═O, as well as by primary amines on the periphery. Anion modes of Li[$(CF_3SO_2)_2N$] are more heavily perturbed in this complex than in the corresponding BPEI or DAB-AM-64 complexes (Table 5). For example, the S−O stretching frequency shifts from 1151 cm^{-1} in Li[$(CF_3SO_2)_2N$] to 1123 cm^{-1} in PAMAM/Li[$(CF_3SO_2)_2N$] (5:1). This 28 cm^{-1} shift is much larger than the shift observed for Li[$(CF_3SO_2)_2N$] in DAB-AM-64-Li[$(CF_3SO_2)_2N$] (9:1) of 12 cm^{-1} (from 1151 to 1139 cm^{-1}).

The N−H stretching frequencies of the amine group in PAMAM are significantly lower than those in the corresponding DAB-AM-64 and BPEI macromolecules, and this difference is attributed to increased hydrogen

(22) Druger, S. D.; Ratner, M. A.; Nitzan, A. *Phys. Rev. B: Condens. Matter* **1985**, *31*, 3939.
(23) Ferry, A.; Doeff, M. M.; De Jonghe, L. C. *J. Electrochem. Soc.* **1998**, *145*, 1586.
(24) Rey, I.; Johansson, P.; Lindgren, J.; Lassegues, J. C.; Grondin, J.; Servant, L. *J. Phys. Chem. A* **1998**, *102*, 3249.
(25) Rey, I.; Lassegues, J. C.; Grondin, J.; Servant, L. *Electrochim. Acta.* **1998**, *43*, 1505.
(26) Colthup, N. B.; Daly, L. H.; Wiberly, S. E. *Introduction to Infrared and Raman Spectroscopy*, 2nd ed.; Academic Press: New York, 1975.
(27) Chatani, Y.; Kobatake, T.; Tadokoro, H.; Tanaka, R. *Macromolecules* **1982**, *15*, 170.

Table 3. FTIR Frequencies and Vibrational Assignments for Anion Modes of Li[$(CF_3SO_2)_2N$] (LiTFSI) Branched and Hyperbranched Polymer Complexes[a] (500−1400 cm^{-1})

FTIR[b]	LiTFSI	A	B	D	E
ν_{as} SO_2[c] (s)	1335	1352, 1333 (w)	1352, 1333 (w)	1352, 1332 (w)	1352, 1332 (w)
ν_{as} CF_3 (vs)	1208	1226 (w), 1191	1226 (w), 1192	1226 (w), 1191	1226 (w), 1193
ν_s SO_2 (m)	1151	1137	1138	1138	1139
ν_{as} SNS (s)	1083, 1068	1058	1058	1059	1059
δ_{as} SO_2 (m)	644	617, 600(w)	617, 600(w)	617, 601(w)	617, 601(w)
δ_{as} CF_3 (m)	575	570	570	571	571

[a] (A) Li[$(CF_3SO_2)_2N$]/BPEI = 1:29. (B) Li[$(CF_3SO_2)_2N$]/BPEI = 1:15. (C) Li[$(CF_3SO_2)_2N$]/BPEI = 1:4 (the quality of these spectra is poor). (D) Li[$(CF_3SO_2)_2N$]/DAB-AM-64 = 1:17. (E) Li[$(CF_3SO_2)_2N$]/DAB-AM-64 = 1:9. (F) Li[$(CF_3SO_2)_2N$]/DAB-AM-64 = 1:4. [b] Assignments: v (stretch), δ (bend). Subscripts as and s denote asymmetric and symmetric motions, respectively. Band intensities: s (strong), m (medium), w (weak). [c] ν_{as} SO_2 (s) is split into two bands, with the weaker component at the lower frequency. Similarly, ν_{as} CF_3 is split into two bands; however, the weaker component is at the higher frequency.

Table 4. FTIR Frequencies and Vibrational Assignments for C−H and N−H Modes of Li[$(CF_3SO_2)_2N$] (LiTFSI) Branched and Hyperbranched Polymer Complexes[a] (1400−3400 cm^{-1})

FTIR[b]	BPEI	A	B	C
ν_{as} NH (w)	3351	3351	3366	3376
ν_s NH (m)	3282	3281	3308, 3283	3317, 3307
δ NH (sh) overtone	3196	3186	3195	
ν_{as} CH_2 (s)	2933	2934	2935	
ν_s CH_2 (m)	2885, 2813	2888, 2818	2906, 2827	
δ NH (w)	1599	1599	1600	
δ CH_2 (s)	1455	1456	1458	

FTIR[b]	DAB-AM-64	D	E	F
ν_{as} NH (m)	3362	3352	3355	3359
ν_s NH (m)	3283	3298, 3270, 3175	3302, 3265, 3175	3306, 3181
δ NH (sh) overtone	3190			
ν_{as} CH_2 (s)	2934	2939	2941	
ν_s CH_2 (s)	2859, 2801, 2736	2863, 2802, 2735	2867, 2805, 2736	
δ NH (m)	1602	1602	1601	1601
δ CH_2 (m)	1462	1463	1463	1461

[a] (A) Li[$(CF_3SO_2)_2N$]/BPEI = 1:29. (B) Li[$(CF_3SO_2)_2N$]/BPEI = 1:15. (C) Li[$(CF_3SO_2)_2N$]/BPEI = 1:4 (these complexes did not give good spectra). (D) Li[$(CF_3SO_2)_2N$]/DAB-AM-64 = 1:17. (E) Li[$(CF_3SO_2)_2N$]/DAB-AM-64 = 1:9. (F) Li[$(CF_3SO_2)_2N$]/DAB-AM-64 = 1:4 (these complexes did not give good spectra). [b] Assignments: v (stretch), δ (bend). Subscripts as and s denote asymmetric and symmetric motions, respectively. Band intensities: s (strong), m (medium), w (weak), sh (shoulder).

Table 5. FTIR Frequencies and Vibrational Assignments for Li[$(CF_3SO_2)_2N$] (LiTFSI) PAMAM Complexes[a] (500−3400 cm^{-1})

FTIR[b]	LiTFSI	G	H	I
ν_{as} CF_3 (sh)	1208	1179	1170	1184
ν_s SO_2 (s)	1151	1123	1123	1125
ν_{as} SNS (m)	1083, 1068	1058	1057	1059
δ_{as} SO_2 (m)	644	618	617, 599	618
δ_{as} CF_3 (w)	575	570	570	573

FTIR[b]	PAMAM	G	H	I
ν_s NH (s)	3280	3283	3381, 3282	3389, 3312
ν_s NH (s)	3068	3192	3193	3192
ν_s C=O (w)	1650	1652	1648	1655
δ NH (w)	1548	1536	1540	1555

[a] (G) Li[$(CF_3SO_2)_2N$]/PAMAM = 1:9. (H) Li[$(CF_3SO_2)_2N$]/PAMAM = 1:5. (I) Li[$(CF_3SO_2)_2N$]/PAMAM = 1:1. [b] Assignments: v (stretch), δ (bend). Subscripts as and s denote asymmetric and symmetric motions, respectively. Band intensities: s (strong), m (medium), w (weak), sh (shoulder).

bonding in PAMAM owing to the presence of the amide group. The dissolution of Li[$(CF_3SO_2)_2N$] into PAMAM results in the N−H symmetric and asymmetric bands shifting to higher frequencies (the asymmetric bands are split at high salt concentrations). The carbonyl stretching frequency does not display a consistent trend with the increasing salt concentration.

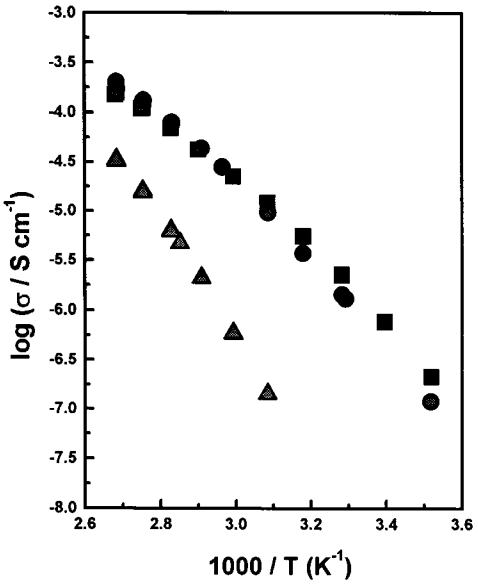

Figure 3. Temperature-dependent conductivities (σ) of BPEI and Li[$(CF_3SO_2)_2N$]: (■) BPEI/Li[$(CF_3SO_2)_2N$] (29:1), (●) BPEI/Li[$(CF_3SO_2)_2N$] (15:1), (▲) BPEI/Li[$(CF_3SO_2)_2N$] (4:1).

Ionic Conductivity. The temperature-dependent ionic conductivities of the amorphous electrolytes formed between BPEI and Li[$(CF_3SO_2)_2N$] (Figure 3) and between DAB-AM-64 and Li[$(CF_3SO_2)_2N$] (Figure 4) can be fit by the semiempirical Vogel−Tamman−Fulcher (VTF) function (eq 1), which is characteristic of systems in which ion motion is coupled to motions of the viscous medium.[28−30]

$$\sigma = AT^{-0.5} \exp[-B/(T - T_o)] \qquad (1)$$

where T_o is a parameter related to the glass transition temperature of the polymer salt complex ($T_o \approx T_g - 50$ °C); B is a pseudo-activation energy term related to the fluctuations in the electrolyte matrix that facilitate ion migration; and the preexponential factor, A, is dependent on the concentration of charge carriers in the matrix. The VTF parameters for the BPEI/Li[$(CF_3SO_2)_2N$] and DAB-AM-64/Li[$(CF_3SO_2)_2N$] complexes are reported in Table 6.

(28) Vogel, H. *Phys. Z.* **1921**, *22*, 645.
(29) Tamman, G.; Heese, W. *Z. Anorg. Allg. Chem.* **1926**, *156*, 245.
(30) Fulcher, G. S. *J. Am. Ceram. Soc.* **1925**, *8*, 339.

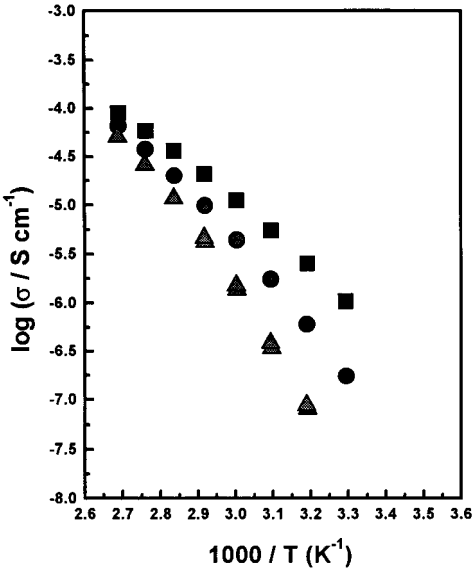

Figure 4. Temperature-dependent conductivities (σ) of DAB-AM-64 and Li[$(CF_3SO_2)_2N$]: (■) DAB-AM-64/Li[$(CF_3SO_2)_2N$] (17:1), (●) DAB-AM-64/Li[$(CF_3SO_2)_2N$] (9:1), (▲) DAB-AM-64/Li[$(CF_3SO_2)_2N$] (4.5:1).

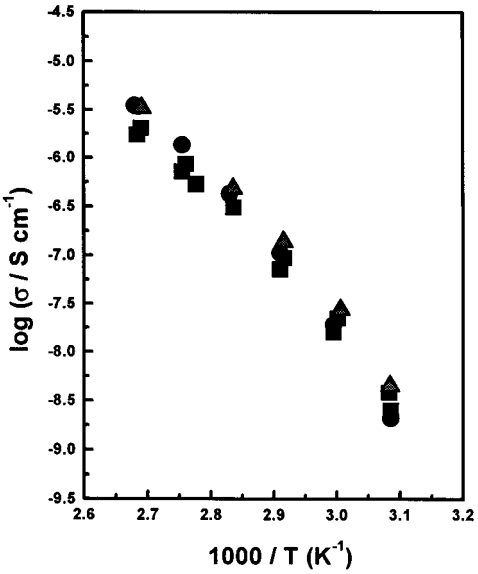

Figure 5. Temperature-dependent conductivities (σ) of PAMAM and Li[$(CF_3SO_2)_2N$]: (■) PAMAM/Li[$(CF_3SO_2)_2N$] (9:1), (●) PAMAM/Li[$(CF_3SO_2)_2N$] (5:1), (▲) PAMAM/Li[$(CF_3SO_2)_2N$] (1:1).

Table 6. VTF Parameters for DAB-AM-64 and BPEI Complexes

complex	A (S K$^{1/2}$ cm^{-1})	B (K)	$T_g - 50 \approx T_o$ (K)
193A	0.0169	630.12	239.15
193B	0.0236	592.27	250.15
193C[a]	0.0031	318.79	303.15
194A	0.0171	703.49	237.15
194B	0.0101	537.01	265.15
194C[a]	0.0023	273.19	300.15

[a] Do not fit the VTF equation well.

The crystalline electrolytes formed between PAMAM and Li[$(CF_3SO_2)_2N$] (Figure 5) can be fit by the Arrhenius equation (eq 2), which indicates that simple hopping prevails in this more-ordered material.

$$\sigma = A \exp[-E_a/RT] \quad (2)$$

The conductivities of BPEI/Li[$(CF_3SO_2)_2N$] (29:1) and BPEI/Li[$(CF_3SO_2)_2N$] (15:1) are almost identical (Figure 3). This observation indicates that the higher concentration of charge carriers might offset the increase in the glass transition temperature as more Li[$(CF_3SO_2)_2N$] is added to BPEI. The ionic conductivity of the DAB-AM-64 complexes (Figure 4) is characteristic of polymer salt complexes, in that the addition of salt results in a lower ionic conductivity and an increasing glass transition temperature. The conductivity plot for PAMAM complexes (Figure 5) parallels the DSC data, which indicate little difference in the crystallinities of these complexes.

Conclusions

Dendrimers are promising hosts for the formation of amorphous alkali metal salt electrolytes. The dendrimer DAB-AM-64 forms more-conducting electrolytes with Li[$(CF_3SO_2)_2N$] than similar complexes with the dendrimer PAMAM. At low salt doping, the ionic conductivity and glass transition temperature of DAB-AM-64 are more favorable than those of BPEI electrolytes. However, at higher concentrations of Li[$(CF_3SO_2)_2N$], the ionic conductivities and glass transition temperatures of both electrolytes are similar. These trends are attributed to the reduced motion of the dendrimer upon coordination of the lithium cation with the primary nitrogen atoms on the periphery of the dendrimer DAB-AM-64.

Acknowledgment. This research was supported by the MRSEC program of the National Science Foundation (DMR-9632472) at the Materials Research Center of Northwestern University.

CM0008866